

Communication

Non-Destructive Monitoring via Electrochemical NADH Detection in Murine Cells

Ju Kyung Lee ¹, Han Na Suh ², Sung Hoon Yoon ^{2,3}, Kyu Hong Lee ², Sae Young Ahn ^{4,5}, Hyung Jin Kim ⁶ and Sang Hee Kim ^{1,*}

¹ Department of Medical IT Convergence, Kumoh National Institute of Technology, Gumi 39177, Korea; chejueyes@kumoh.ac.kr

² Korea Institute of Toxicology, Jeongeup 56212, Korea; hanna.suh@kitox.re.kr (H.N.S.); seonghoon.yoon@kitox.re.kr (S.H.Y.); khlee@kitox.re.kr (K.H.L.)

³ Department of Human and Environmental Toxicology, University of Science & Technology, Daejeon 34113, Korea

⁴ NDD Inc., Gumi 39253, Korea; sahn@n-dd-inc.com

⁵ Fuzbien Technology Institute, Rockville, MD 20850, USA

⁶ Digital Health Care Research Center, Gumi Electronics and Information Technology Research Institute (GERI), Gumi 39253, Korea; hjkim745@geri.re.kr

* Correspondence: shkim@kumoh.ac.kr

Abstract: Nicotinamide adenine dinucleotide (NADH) is an important cofactor involved in metabolic redox reactions in living cells. The detection of NADH in living animal cells is a challenge. We developed a one-step monitoring method for NADH via an electrocatalytic reaction that uses a surface-modified, screen-printed electrode (SPE) having a redox active monolayer 4'-mercapto-N-phenylquinone diamine (NPQD) formed by a self-assembled monolayer (SAM) of an aromatic thiol, 4-aminothiophenol (4-ATP). This electrode has a limit of detection (LOD) of 0.49 μM and a sensitivity of $0.0076 \pm 0.0006 \mu\text{M}/\mu\text{A}$ in cell culture media, which indicates that it retains its selectivity. The applicability of this NADH sensor was demonstrated for the first time by cell viability monitoring via NADH-sensing in cell culture supernatants.

Keywords: electrochemical amperometry; surface modification; screen-printed electrode (SPE); polyhexamethylene guanidine-phosphate (PHMG-p); continuous monitoring



Citation: Lee, J.K.; Suh, H.N.; Yoon, S.H.; Lee, K.H.; Ahn, S.Y.; Kim, H.J.; Kim, S.H. Non-Destructive Monitoring via Electrochemical NADH Detection in Murine Cells. *Biosensors* **2022**, *12*, 107. <https://doi.org/10.3390/bios12020107>

Received: 4 January 2022

Accepted: 8 February 2022

Published: 10 February 2022

Publisher's Note: MDPI stays neutral with regard to jurisdictional claims in published maps and institutional affiliations.



Copyright: © 2022 by the authors. Licensee MDPI, Basel, Switzerland. This article is an open access article distributed under the terms and conditions of the Creative Commons Attribution (CC BY) license (<https://creativecommons.org/licenses/by/4.0/>).

1. Introduction

Nicotinamide adenine dinucleotide (NADH) is the most well-known biomarker of the redox state of a cell. Several studies have reported that a deficiency of NADH causes a metabolic state problem due to a lack of ATP because ATP production depends on the redox state of coenzymes and NADH. Additionally, mitochondrial dysfunction characterized by inefficient ATP production contributes to neurodegenerative diseases, such as Alzheimer's, Parkinson's, and Huntington's diseases, cardiovascular disease [1,2], diabetes and metabolic syndrome [3–5], and lung diseases [6,7]. For these reasons, intracellular NADH has a diagnostic potential as a biomarker for cellular redox reactions, energy production, and mitochondrial functions; therefore, it is important to quantify NADH correctly in in vitro study.

Many studies present various quantification methods for NADH because it exists in cells at a higher concentration than other coenzymes, and its quantification is not affected significantly by blood [8]. Additionally, Adriouch et al. reported that NAD⁺ released during inflammation participates in T-cell homeostasis by inducing the ART2-mediated death of naive T-cells in biogel polyacrylamide bead-induced lung inflammation [9]. The classical method for the determination of NADH is an optical assay using absorbance [10] or fluorescence [11] and a colorimeter [12]. Some classical methods are robust, standardized analytical methods to determine NADH, but they require a colorimeter, which occupies a

great deal of space and has a high sample volume (~200 μL) and a high cost per test. An electrochemical (EC) biosensor for NADH has emerged as an alternative to the classical method because it has several advantages, such as convenience and a short analysis time; furthermore, it uses a small sample volume while maintaining high sensitivity and selectivity. These types of sensors use the oxidation/reduction reaction of the NADH/NAD⁺ couplet at a specific potential.

In this research, we developed a screen-printed electrode (SPE) as a substrate, and 4'-mercapto-N-phenylquinone diamine (NPQD) as an electrocatalyst was immobilized by double-step electrochemical functionalization. This NPQD layer can be constructed via the functionalization of 4-aminothiophenol (4-ATP), which was previously immobilized on the Au layer by covalent bonding based on Au-thiol bonding as initially developed by the Takeo group [13]. Although NPQD functionalization is similar, we selected a different electrochemical functionalization method and used a different substrate as the SPE. The limit of detection (LOD) and sensitivity was improved compared with the previous result. Also, we investigated the electrocatalytic reaction in cell culture media to detect NADH in viable cells and observed NADH level by inserting toxicological material to induce cell death. As mentioned above, NADH produced in the mitochondria is an important biomarker for metabolic activity and mitochondrial function, and it is also useful as a biomarker for monitoring living cells because mitochondria lose their functionality after cell death. The reliability of the electrochemical results was compared with that of a conventional WST-1 (water-soluble tetrazolium salt-1) assay, and the two reliabilities were found to be similar. Finally, we challenged the NADH electrochemical sensor with cell culture medium and observed that it performed well in further *ex vivo* experiments. PHMG-p (Polyhexamethylene guanidine-phosphate) was used as toxic material which induced cell death, and the NADH was quantified and compared via a control model. To the best of our knowledge, this study is the first attempt to quantify NADH electrochemically *in vitro*, and we believe that this sensor can be used for NADH detection for disease diagnosis and the continuous monitoring of mitochondrial function.

2. Materials and Methods

2.1. Chemicals

A premixed WST-1 cell proliferation assay kit was purchased from Takara Bio Inc. (Katsu, Japan). RPMI 1640 medium and penicillin-streptomycin were purchased from Life Technologies Co. (New York, NY, USA). Polyhexamethylene guanidine-phosphate (PHMG-p) was provided by SK chemicals (Seongnam, Korea). Potassium ferricyanide [$\text{K}_3\text{Fe}(\text{CN})_6$], 4-aminothiophenol (4-ATP), 100 mM and 10 mM of Dulbecco's phosphate buffered saline (DPBS), Tween 20, and absolute ethanol were purchased from Sigma-Aldrich (St. Louis, MO, USA) and used without further purification. All reagents used in the investigation were of analytical grade.

2.2. Apparatus and Electrode

Commercial screen-printed electrodes (SPE, Model No: DRP 220 AT, $\Phi = 4$ mm), including a Au working electrode (WE) with a surface area of 12.56 mm², were purchased from the Metrohm DropSens Co. (Oviedo, Spain). This electrode includes a Au counter electrode (CE) and a silver pseudo-reference electrode (RE). Chronoamperometry (CA) and cyclic voltammetry (CV) measurements were conducted with a multi-channel potentiostat obtained from CH instruments (Texas, TX, USA, Model No: CH 1030C) and Wismar Co. Ltd. (Daejeon, Korea, Model No: WIZECM-1200Premium). Electrochemical impedance spectroscopy (EIS) was carried out with a pocketSTAT from Ivium Technologies B.V. (AJ Eindhoven, The Netherlands). All electrochemical (EC) measurements were conducted at room temperature in a Faraday cage.

2.3. Surface Modification of the SPE

Prior to assembly, the SPE was pretreated by placing a 50 μL drop of a 10 mM H_2SO_4 solution on it, and cyclic voltammetry was performed from 0 V to 1.8 V at a scan rate of 100 mV/s to remove dust. The SPE was then washed with DI water and dried with nitrogen. After drying in a stream of N_2 , the 4-ATP self-assembled monolayer (SAM) was prepared on the SPE by incubating the electrode in 10 mM 4-ATP dissolved in absolute ethanol for 2 h at room temperature as mentioned by the Takeo group [13]. Then, the SPE was washed with absolute ethanol for 1 min and washed again with 0.05% Tween 20 in 10 mM DPBS (pH 7.2) to remove the remaining chemicals. A 4'-mercapto-N-phenylquinone diamine (NPQD) layer was generated on the Au electrode by a two-step electrochemical surface modification. After drying in a stream of N_2 , 50 μL of 100 mM DPBS (pH 7.2) was dropped on the SPE, and CV was performed by applying a potential between 0.8 V and -0.4 V 30 times. After washing the electrode using 10 mM DPBS (pH 7.2), a CV step similar with that conducted in the previous step was performed again by changing the 100 mM DPBS to 10 mM DPBS. After a surface modification, the electrode was washed with 0.05% Tween 20 in 10 mM DPBS and kept in 10 mM DPBS.

2.4. In Vitro Studies

2.4.1. Cell Culture and WST-1 Viability Assay

Human epithelial (A549) cells from the American Type Culture Collection (Manassas, VA, USA) were cultured to confluence in culture media (pH 7.2) with 5% FBS and 100 IU/mL penicillin–streptomycin at 37 °C in a humidified atmosphere containing 95% air and 5% CO_2 . Suspensions of A549 Cells (2×10^5 cells/well) were transferred to separate well plates after an overnight incubation at 37 °C in 5% CO_2 . The cytotoxicity of PHMG-p was evaluated versus concentration and time. To investigate the cytotoxicity of the PHMG-p, cells were seeded in a 6-well plate and exposed to increasing concentrations of PHMG-p (i.e., 1.0, 2.0, 3.0, 4.0, and 12.5 $\mu\text{g}/\text{mL}$) for 6, 12, or 24 h. On another plate, the time course effect of PHMG-p was investigated by seeding cells, exposing them to 4 and 8 $\mu\text{g}/\text{mL}$ of PHMG-p, and monitoring them for 6, 12, 24, or 36 h. Three replicates were used at each concentration. Cells not treated with PHMG-p were used as the positive control, and media (no cells) was used as the negative control. In both experiments, cell viability was monitored by a WST-1 assay. Prior to adding the WST-1 reagent to the plate, 200 μL of the supernatant was extracted from each plate and placed in a 1.5 mL microtube to quantify the NADH in the cell supernatant by an electrocatalytic reaction. After adding the WST-1 to the plate, the plate was placed in an incubator at 37 °C and 5% CO_2 for 1 h. The absorbance of each well was measured at 450 nm in a microplate reader. The relative cell viability percentage in each group was calculated by comparing the cell viability in each group to that of the control group.

2.4.2. Quantification of NADH in Cell Supernatants

To quantify the NADH in the cell culture supernatants, 50 μL of the supernatant extracted as described in the previous section was added dropwise to the NPQD-modified electrode. NADH quantification was performed within 10 min of extraction to prevent contamination. Three replicates were used at each concentration, non-treated PHMG-p cells were used as the positive control group, and media (no cells) were used as the negative control. As previously mentioned, we applied a potential of 0.7 V and read the current after 20 s, when it had achieved a stable state.

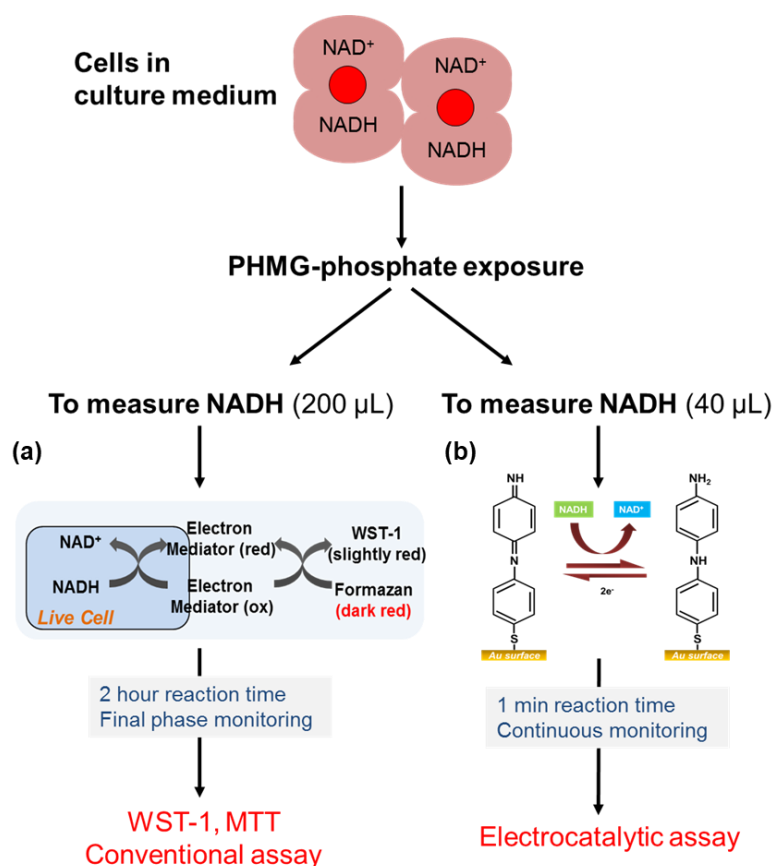
2.5. Statistical Analysis

All values were expressed as the mean \pm standard deviation. Statistical analyses were performed using a two-tailed *t*-test. Statistical significance was defined as $p < 0.05$. All assays were run five times and mean and standard deviation were calculated at each concentration to generate the calibration curve. Each replicate was measured with a new

screen-printed electrode. The analyte NADH was newly made at each time measurement to maintain fresh conditions. Linear curve fitting was performed with the Origin 8.0 program.

3. Results and Discussion

Many important aspects of the metabolic state of the mitochondria can be evaluated by monitoring the NADH in the cell in terms of energy production and intracellular oxygen levels [14]. MTT (3-(4,5-dimethylthiazol-2-yl)-2,5-diphenyltetrazolium bromide) and WST-1 (water soluble tetrazolium salt-1) analysis is widely used for cell viability via NADH detection (Scheme 1a). A549 cells were seeded in 6-well or 12-well plates and incubated for 24 h. Additionally, the cells were treated with PHMG-p. After the cells were incubated for 6, 12, and 24 h to observe the time effect induced by PHMG-p, the supernatant was collected. A collected sample was used for WST-1, MTT, and electrocatalytic analysis. We further investigated whether our electrocatalytic sensor could detect NADH to monitor mitochondrial dysfunction in an *in vitro* cell culture system. To achieve this, the NADH electrocatalytic sensor was used in a cell viability assay to determine the number of viable cells after a defined incubation period [15]. Scheme 1b shows a schematic illustration of the formation of the NPQD layer for the electrocatalytic reaction of NADH. The substance 4'-mercapto-N-phenylquinone diamine (NPQD) was chosen as the electrocatalyst and immobilized by electrochemical functionalization due to its good redox behavior and rigid structure [13]. In addition, it lowers the oxidation potential and enhances the current because diamines are electroactive, easily oxidized, and can transfer two electrons via NADH oxidation to NAD^+ (one electron transfer).



Scheme 1. Schematic illustration of the electrocatalytic cell viability assay: (a) Conventional WST-1 or MTT assay based on optical method; (b) Electrocatalytic assay based on electrochemical method.

The NPQD layer can be constructed via the electrochemical functionalization of 4-ATP (4-aminothiophenol) which was previously immobilized by covalent bonding as first devel-

oped by the Takeo group. In this paper, NPQD was generated with a similar process but a different electrochemical functionalization method to improve the performance. Figure 1a shows the CV (cyclic voltammogram) data as obtained during the functionalization of 4-ATP in 100 mM PBS buffer (pH 7.2). This result is similar but different from that in previous reports because the cathodic current at 0.55 V and the anodic current at -0.2 V decreased and the reversible redox peak at 0.23 V newly emerged via a repeating CV cycle. However, the redox peak at 0.23 V was not observed, and we speculated that this was due to differences in our proposed system. The SPE consists of Au working, Au counter, and Ag reference electrodes, and 4-ATP was immobilized on the working electrode and on the counter electrode. This caused electrochemical motion in a manner different from that in previous reports because only the Au working electrode, and not the counter electrode, was functionalized. Given that the repeated CV signal in 100 mM PBS buffer is unstable, we performed a “double-step” electrochemical functionalization using a low concentration of PBS buffer (10 mM con, pH 7.4) after a high concentration PBS buffer for stabilization while maintaining other CV parameters. Although the current, approximately corresponding to -0.4 V, did not exhibit significant fluctuation, changes observed in the high concentration were not observed in the 10 mM PBS buffer as shown in Figure 1b.

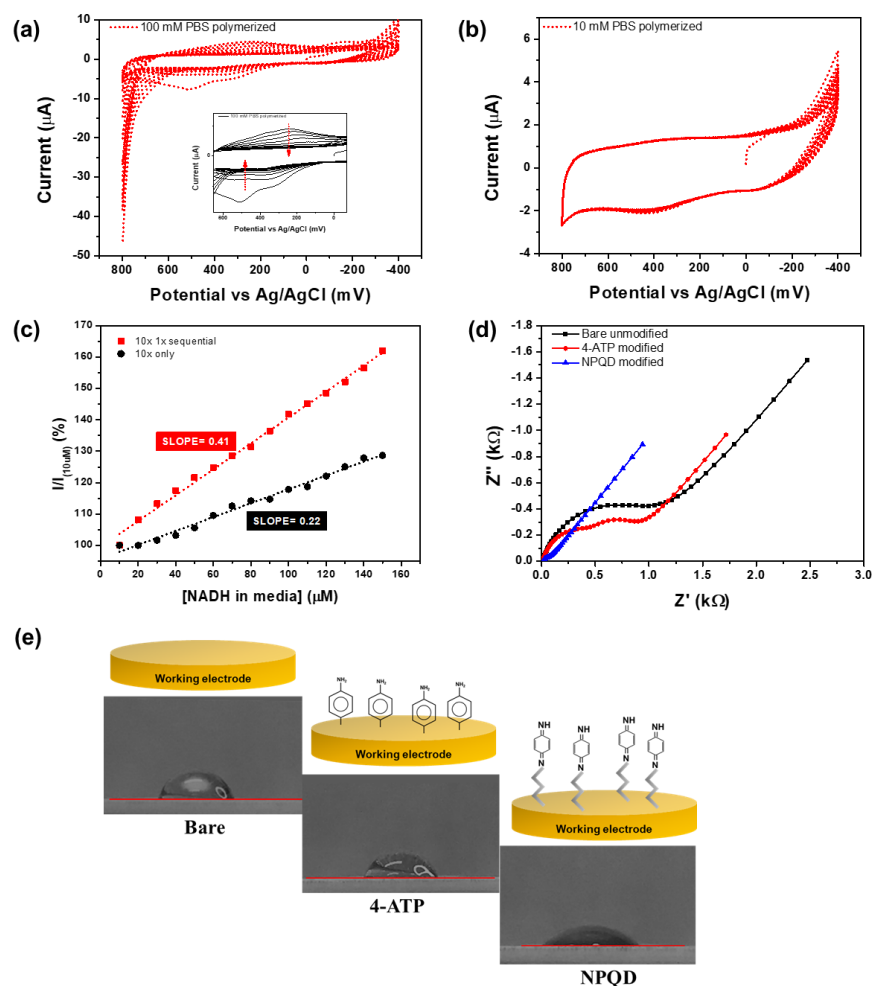


Figure 1. CV data during the electrochemical functionalization of the 4-ATP-Au electrode in: (a) a 100 mM PBS (pH 7.4); and (b) 10 mM PBS (pH 7.4) after (a). The scan rate is 100 mV/s; (c) NADH detection with double-step polymerized and single polymerized; (d) Nyquist plot of each electrode; (e) contact angle measurement of each electrode.

The NADH-sensing performance of the single-step electrochemical functionalization using 100 mM PBS buffer and double-step electrochemical functionalization sequentially using 100 mM and 10 mM PBS buffer are shown in Figure 1c. The red line is the double-step electrode's performance, and the slope is 0.41, and the black line is the single-step electrode's performance, and the slope is 0.22, respectively. We found the slope (sensitivity) was improved two times, compared with the previous method. Also, the LOD value of the double-step polymerized reaction had 494 nM, and a single-step polymerized reaction is 1.4 μ M. We found that the LOD and sensitivity were improved compared with previous method. As a result, correct quantitative measurement is possible.

As shown in the Figure 1d, EIS (electrochemical impedance spectroscopy) was used to investigate unmodified 4-ATP- and NPQD-modified Au surfaces at a constant concentration of redox species of $\text{Fe}(\text{CN})_6^{3-/4-}$, and we found a charge-transfer resistance (R_{ct}) that was expressed by the diameter of a semicircle in a Nyquist plot of the NPQD-modified surface, which had a minimum value (63.79 k Ω) compared with the unmodified and ATP-modified electrodes (1041 k Ω and 583.4 k Ω , respectively). Additionally, a 45° line in the Nyquist plot indicates a Warburg region of semi-infinite diffusion of a species in the modified electrode, and the NPQD-modified electrode clearly shows a diffusion process governed by the mass transport of the redox molecules from the solution to the electrode. NPQD functionalization was also demonstrated by the contact angle measurement of a water droplet and EDAX analysis because the -NH functional group in NPQD is polarized and hydrophilic. As shown in Figure 1e, the contact angle of the bare electrode was 63.4°, and for the 4-ATP modified electrode, it was 56.9°, a value not much different from that of the bare electrode. However, the NPQD-modified electrode showed a much lower value of 34.9° due to the amine group of NPQD. EDAX images also confirm the stepwise modification [16] (see Supplementary Materials, Figure S1).

Figure 2a–c depicts the cyclic voltammetry and chronoamperometry demonstrating the electrocatalytic activity of the NPQD-Au electrode for NADH oxidation in medium buffer. A cyclic voltammogram from –100 mV to 700 mV shows that the current did not change until 400 mV when NADH was added. However, a dramatic enhancement of anodic current began from the 400 mV higher potential range when NADH was added. This current was caused by NADH oxidation to NAD^+ , which regenerates the diamine, as shown in the schematic in Figure 1. To oxidize NADH to NAD^+ , a potential is required as the driving force, and we found that the minimum potential for oxidation is 400 mV. Next, we constructed a calibration plot of NADH at various potentials found from cyclic voltammetry (400, 500, 600, and 700 mV), and the 600 mV results showed the widest sensitivity range and linear range. Chronoamperometry was used to make a calibration plot of NADH, and a short, fixed potential analysis time (10 s) per sample was required, compared with cyclic voltammetry [17,18]. A plot of the steady current at 10 s vs. the NADH concentration followed the adjusted equation $I \text{ (nA)} = \{-5.67\} \cdot [\text{NADH}], \mu\text{M} - 13.64$ ($R^2 = 0.999$), with a range of linearity between 1.8–1000 μ M and had a 250 nM of LOD (limit of detection). The LOD value was calculated from the measurements carried out with three different NADH sensors for each concentration. The achieved sensitivity and sensing range was applicable to cell studies and non-clinical animal experiments, such as those conducted on mice, because the known concentrations in animal cells are approximately 0.3 mM [8,19].

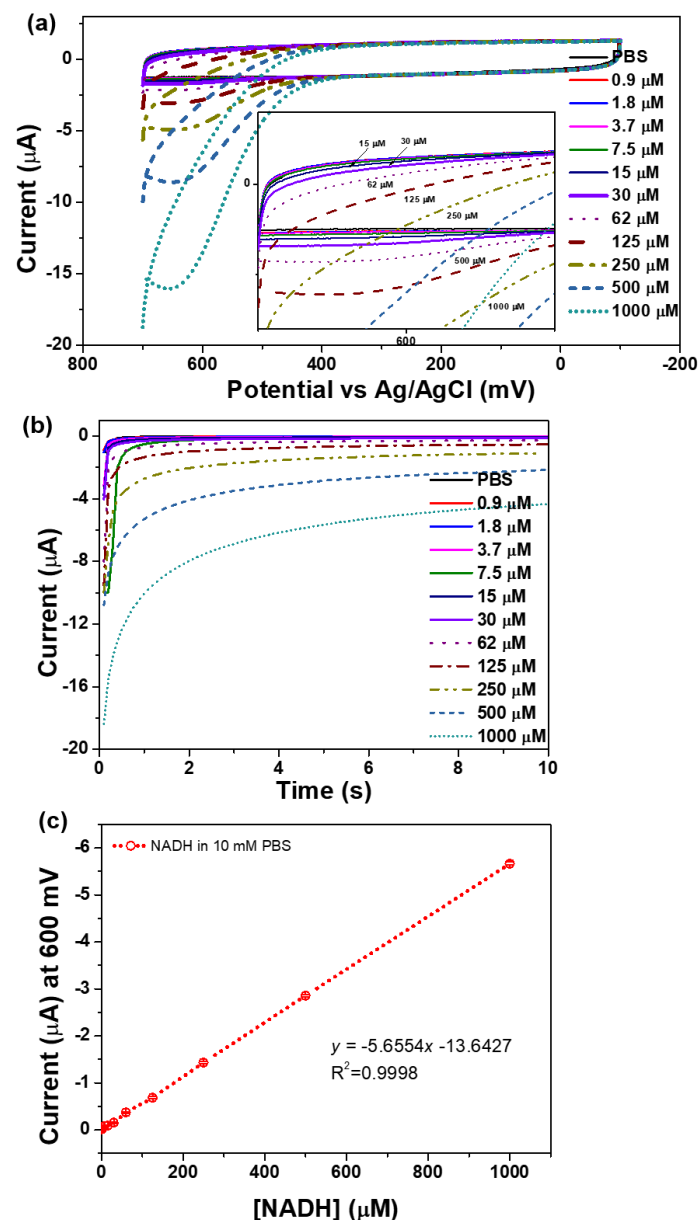


Figure 2. Typical electrochemical results for NADH in medium: (a) cyclic voltammogram; (b) chronoamperometry; and (c) calibration plot of NADH in medium ($n = 5$).

The viability obtained by the WST-1 assay depends on the number of live cells, as they use the product formazan, which is generated by mitochondrial dehydrogenases in live cells. However, viability is determined differently with the EC (electrocatalytic) and WST-1 assays. We hypothesized that measured NADH would greatly increase directly after cell death. Cell viability was calculated by the following Equations (1) and (2).

$$\text{Cell viability}_{\text{EC}} (\%) = 100 - (\text{VF}_{\text{EC}}) = 100 - \left(\frac{I_s - I_c - I_0}{I_c - I_0} \times 100 \right) \quad (1)$$

Equation (1): Cell viability by the electrocatalytic assay: I_s is the current value of a sample treated with a specific concentration of PHMG-p, I_c is the current value of the control sample that was not treated with PHMG-p, and I_0 is the current value of the blank.

VF_{EC} is the viability factor by electrocatalytic reaction. All current was measured at a 600 mV potential.

$$\text{Cell viability}_{\text{WST-1}} (\%) = \left(\frac{A_s - A_b}{A_c - A_b} \right) \times 100 \quad (2)$$

Equation (2): Cell viability by the WST-1 assay. A_s is the optical density at 450 nm of a sample treated with a specific concentration of PHMG-p (cells treated with PHMG-p+WST-1), A_c is the optical density of the control sample that was not treated with PHMG-p (the cells were not treated with PHMG-p+WST-1), and A_b is the optical density of the blank (WST-1). All measurements were performed in the cell culture medium.

To test this hypothesis, the cytotoxic effect of PHMG on A549 cells was evaluated by comparing the electrocatalytic measurements to the results of the WST-1 conventional cell viability assay (Figure 3). Raw data of electrocatalytic reaction and conventional sensing data is shown at Figure S2. Previously, we already established an animal model of PHMG-p-induced lung inflammatory and fibrotic responses and reported that PHMG-p induces polymorphonuclear cells (PMN) and macrophage-dominant lung inflammation during week 1 and marked lung fibrosis from weeks 2 to 10 via histologic analyses of H&E and Masson's trichrome stained preparations [20].

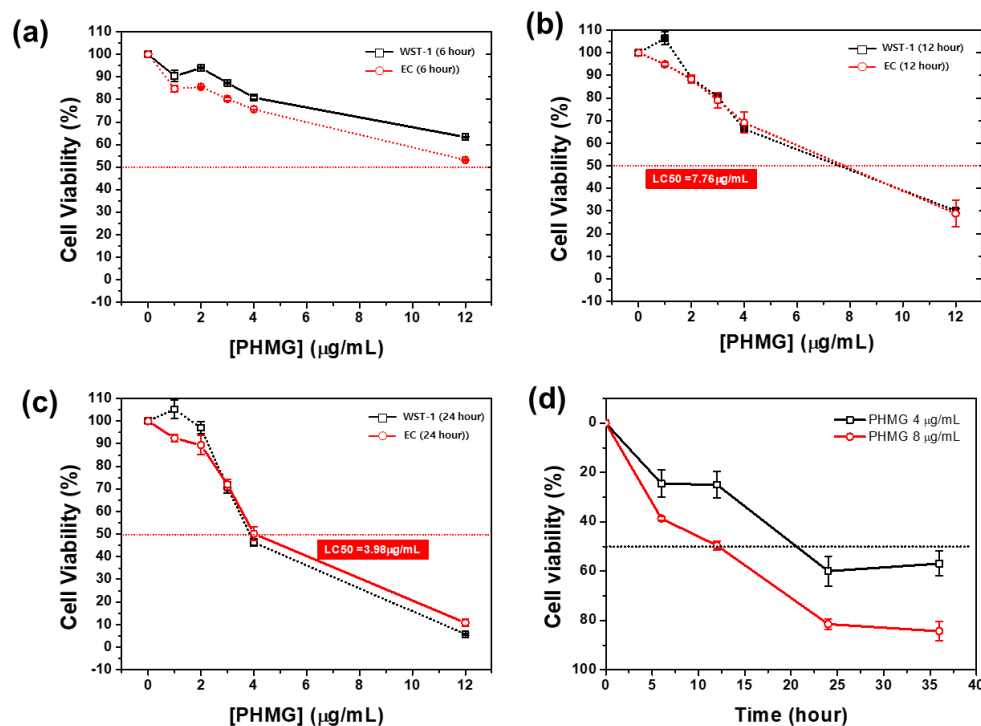


Figure 3. (a) 6-h assay; (b) 12-h assay; (c) 24-h assay; and (d) Continuous cell viability monitoring of PHMG-induced cells ($n = 5$).

First, to understand the effect of PHMG-p concentration on the cells, we performed a cell viability assay with exposure to 1.0, 2.0, 3.0, 4.0, and 12.5 µg/mL PHMG-p. As expected, a decrease in cell viability was observed with an increasing concentration of PHMG-p. It is worth noting that the viability value obtained by the EC assay was similar to that obtained by the WST-1 assay, even though the NADH-sensing approaches in the two assays are different. Another aspect of the EC viability assay is the time-dose effect of PHMG-p. To understand this, the current was measured at 700 mV by using the cell culture media after exposure to 4 µg/mL of PHMG-p. The PHMG-exposure concentration of 4 µg/mL was used because it exhibits the cytotoxic effect more clearly than other concentrations. A comparison with the control revealed that the current value was most significantly increased

after PHMG-exposure time (Figure 4) with fixing PHMG-concentration (4 $\mu\text{g}/\text{mL}$). After 6, 12, and 24 h, the current increased by 21.33 (Figure 4a), 26.03 (Figure 4c), and 46.35% (Figure 4e), respectively, compared with the control. This means that increasing exposure time leads to increased cell death. As shown in Figure 3b,d,f, negative current value was increased with increasing exposure time because NADH was generated when cells die. To fully understand the PHMG-p exposure-time effect, cells were exposed to various concentrations of PHMG-p, and the viability was observed after 6, 12, and 24 h. As shown in Figure 3a–d, a decrease in cell viability with an increasing PHMG-p exposure time was observed in both the WST-1 and EC cell viability assays. The 50% lethal concentration (LC 50) of PHMG-p in the WST-1 and the EC assays was 7.76 $\mu\text{g}/\text{mL}$ at the 12-h exposure time and 3.38 $\mu\text{g}/\text{mL}$ at the 24-h exposure time, respectively (Equations (1) and (2)).

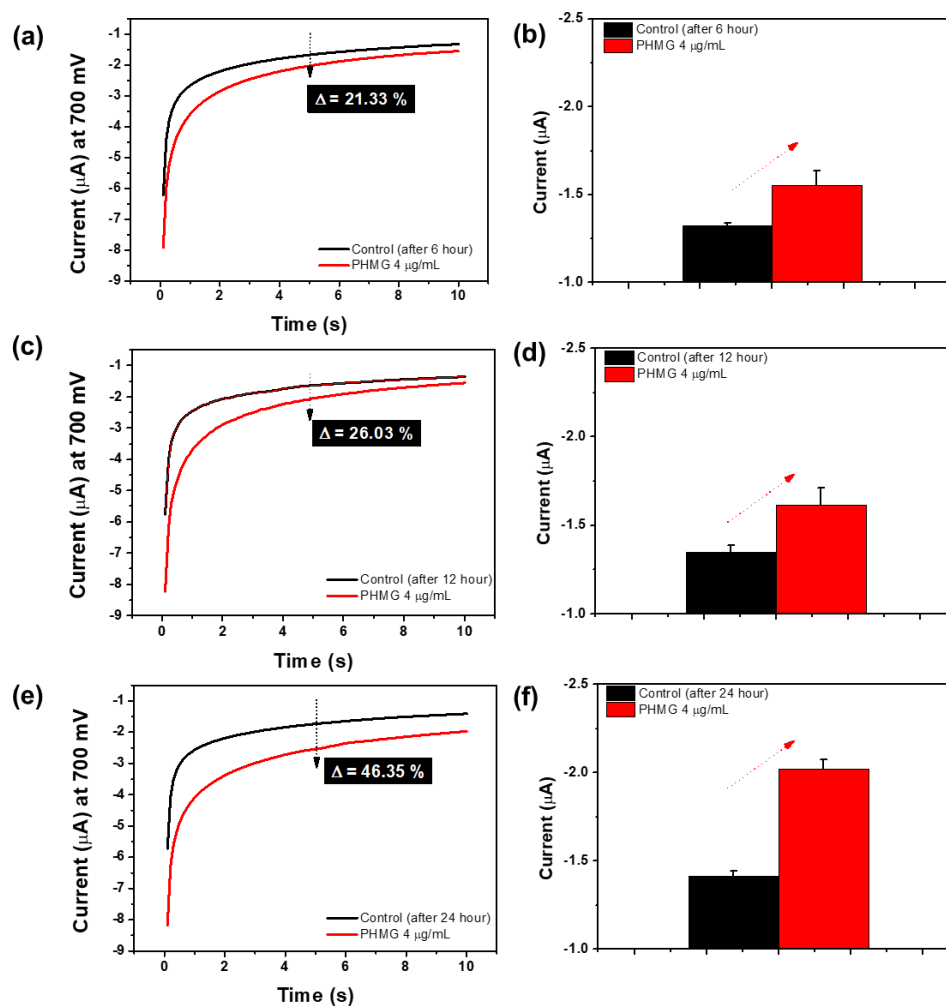


Figure 4. Chronoamperometry measurement of PHMG-induced cells for cell viability monitoring: (a,b) control vs. 6 h; (b,c) control vs. 12 h; (d,e) control vs. 24 h after exposure ($n = 5$).

These data suggest that increased concentrations and exposure times of PHMG-p result in reduced cell viability. This viability was measured by the EC assay, and the result was similar to that obtained with the WST-1 conventional assay. The greatest advantage of the EC assay is that cell viability can be measured continuously, as the EC assay does not require chemicals, such as tetrazolium salts; therefore, the samples are not damaged as in the WST-1 conventional assay. To verify these results, continuous monitoring of cell viability was performed by the EC assay after exposure to 4 and 8 $\mu\text{g}/\text{mL}$ of PHMG-p (Figure 3d). The cell viability after exposure to both concentrations decreased, but the results for 8 $\mu\text{g}/\text{mL}$ showed a lower cell viability than those for 4 $\mu\text{g}/\text{mL}$. The lethal time

(LT 50) for 4 µg/mL was 23.24 h, and the LT 50 for 8 µg/mL was 12.41 h. These results are similar with the results shown in Figure 3a–d. Taken together, these data strongly suggest that cell viability decreased with an increasing PHMG-p concentration and exposure time, and that our EC assay has the potential to not only replace the conventional cell viability assay, but also to aid in cytotoxicity studies of a variety of toxic materials as continuous cell viability monitoring is also possible. Table 1 presents the many types of sensors to measure NADH used in the past 5 years [21–38]. Our electrocatalytic sensor has the advantages of comprising one simple step, consuming a low volume of sample (50 µL), and having a low LOD. Also, this is the first attempt to use it as a tool to observe the relationship with NADH and cell viability and apply it to toxicological study.

Table 1. Comparison of NADH detection with various analytical methods.

Year	Type	Specific Methods/Material	LOD	Ref.
2017	Electrochemical	Silver nanocluster	22.3 µM	[21]
	Electrochemical	Au–Ag nanoparticles/poly L-cysteine/reduced graphene oxide nanocomposite	1.05 mM	[22]
2018	Electrochemical	Graphical abstract Schematic of the 2D MoSe ₂ /HEG	1 µM	[23]
	Electrochemical	RuO ₂ -GNR/SPCE	0.52 µM	[24]
	Electrochemical	Hierarchically structured PEDOT CMs electrodes	5.3 µM	[25]
2019	Optical	WST-8 and UV spectrophotometric methods	0.32, 1.65 nM	[26]
	Optical	ELISA kit + mBFP protein	2 pM	[27]
	Electrochemical	MWCNTs–CS/GCE electrode	0.12 µM	[28]
	Electrochemical	Frex fluorescence sensor	100 µM	[29]
	Electrochemical	boronic acid functionalized carbon nanodots and poly(thionine) on an electrode surface	0.15 µM	[30]
	Electrochemical	pre-anodized screen-printed carbon electrode	28.9 µM	[31]
	Electrochemical	a dual-signal-output ratiometric ECL sensor	2.5 µM	[32]
2020	Electrochemical	PtAg nanoshells supported on reduced graphene oxide (PtAg/rGO)	0.2 µM	[33]
	Electrochemical	screen-printed CNF electrode	0.5 µM	[34]
2021	Optical	Au80Ag20 NPs	0.23 µg/mL	[35]
	Optical	novel light-controlled colorimetric detection assay	0.27 µg/mL	[36]
	Electrochemical	N-CQDs decorated SnO ₂ /ionic liquid/carbon paste electrode	0.8 nM	[37]
	Electrochemical	SPCE/AuNPs/PMB	0.4 mM	[38]
2022	Electrochemical	SPE/NPQD/double-polymerized electrocatalytic assay	0.45 µM	The present work

Note: HEG: hydrogen exfoliated graphene; SPCE: screen-printed carbon electrode; GNR: graphene nanoribbon; PEDOT: poly(3,4-ethylenedioxythiophen); CM: colloid microparticles; mbfp: metagenome-derived blue fluorescent protein; MWCNT: multiwall carbon nanotube; CS: chitosan; GCE: glassy carbon electrode; Frex: fluorescent reagent; ECL: electrochemiluminescence; N-CQD: N-doped carbon quantum dot; PMB: polymethylene blue.

We have demonstrated that changes in the NADH concentration, as determined by our electrocatalytic sensor, in live cells can be used to monitor cytotoxic events caused by the addition of toxic compounds such as PHMG-p, which provides a framework for toxicity studies for the first time. Such a technique permits the sensing of NADH redox signaling without disrupting or destroying the cells to facilitate the investigation of a complex biological fluid. Individual monitoring via group, continuous, or end-point monitoring are some of the advantages of our electrocatalytic sensor which can improve the understanding of the relationship between NADH and cytotoxic effects. Although further studies are required for an accurate understanding of the mechanism of NADH in

this study, this approach could establish NADH as a potential and important biomarker of cytotoxicity and the electrocatalytic sensor as an efficient assay for NADH concentration.

4. Conclusions

We demonstrated that the developed electrocatalytic sensor enables detection of NADH and can be applied to cell viability with simple devices. To increase the LOD and sensitivity, a double-step polymerized method was used. As a result, the LOD was 0.45 μM and analysis time was 10 s per sample. The sensor was applied to detect cell viability by inserting PHMG-p as toxic matter, and we found that NADH level increased when we inserted a high level of PHMG-p because it caused cell death. This demonstrates that the NADH electrocatalytic sensor will become a powerful tool for cell viability assays and pave the way for toxicological study.

Supplementary Materials: The following supporting information can be downloaded at: <https://www.mdpi.com/article/10.3390/bios12020107/s1>, Figure S1. EDAX spectrum of (a) bare, (b) 4-ATP modified, (c) NPQD modified electrode; Figure S2. The electrocatalytic (a–c) and conventional WST-1 (d–f) sensing data for cell viability monitoring. PHMG was dosed for 6 h (a,d), for 12 h (b,e), for 24 h (c,f).

Author Contributions: J.K.L. and H.N.S. contributed equally to this work. J.K.L. wrote the main manuscript and performed overall experiments. H.N.S. and S.H.Y. performed cell experiments using PHMG. S.Y.A. performed the electrochemical experiment. K.H.L., H.J.K., and S.H.K. directed the paper. All authors have read and agreed to the published version of the manuscript.

Funding: This research was supported by research fund of Kumoh National Institute of Technology (2019-104-044).

Data Availability Statement: Not applicable.

Conflicts of Interest: The authors declare no conflict of interest.

References

1. Victor, V.M.; Apostolova, N.; Herance, R.; Hernandez-Mijares, A.; Rocha, M. Oxidative stress and mitochondrial dysfunction in atherosclerosis: Mitochondria-targeted antioxidants as potential therapy. *Curr. Med. Chem.* **2009**, *16*, 4654–4667. [[CrossRef](#)] [[PubMed](#)]
2. Limongelli, G.; Masarone, D.; D'Alessandro, R.; Elliott, P.M. Mitochondrial diseases and the heart: An overview of molecular basis, diagnosis, treatment and clinical course. *Future Cardiol.* **2012**, *8*, 71–88. [[CrossRef](#)]
3. Ma, Z.A.; Zhao, Z.; Turk, J. Mitochondrial dysfunction and β -cell failure in type 2 diabetes mellitus. *Exp. Diabetes Res.* **2011**, *2012*, 703538. [[CrossRef](#)] [[PubMed](#)]
4. Joseph, A.M.; Joannis, D.R.; Baillot, R.G.; Hood, D.A. Mitochondrial dysregulation in the pathogenesis of diabetes: Potential for mitochondrial biogenesis-mediated interventions. *Exp. Diabetes Res.* **2011**, *2012*, 642038. [[CrossRef](#)] [[PubMed](#)]
5. Nicolson, G.L. Metabolic syndrome and mitochondrial function: Molecular replacement and antioxidant supplements to prevent membrane peroxidation and restore mitochondrial function. *J. Cell. Biochem.* **2007**, *100*, 1352–1369. [[CrossRef](#)] [[PubMed](#)]
6. Kim, S.R.; Kim, D.I.; Kim, S.H.; Lee, H.; Lee, K.S.; Cho, S.H.; Lee, Y.C. NLRP3 inflammasome activation by mitochondrial ROS in bronchial epithelial cells is required for allergic inflammation. *Cell Death Dis.* **2014**, *5*, e1498. [[CrossRef](#)]
7. Marshall, J.D.; Bazan, I.; Zhang, Y.; Fares, W.H.; Lee, P.J. Mitochondrial dysfunction and pulmonary hypertension: Cause, effect, or both. *Am. J. Physiol. Lung Cell. Mol. Physiol.* **2018**, *314*, L782–L796. [[CrossRef](#)]
8. Yang, H.; Yang, T.; Baur, J.A.; Perez, E.; Matsui, T.; Carmona, J.J.; Lamming, D.W.; Souza-Pinto, N.C.; Bohr, V.A.; Rosenzweig, A.; et al. Nutrient-sensitive mitochondrial NAD⁺ levels dictate cell survival. *Cell* **2007**, *130*, 1095–1107. [[CrossRef](#)]
9. Adriouch, S.; Hubert, S.; Pechberty, S.; Koch-Nolte, F.; Haag, F.; Seman, M. NAD⁺ released during inflammation participates in T cell homeostasis by inducing ART2-mediated death of naive T cells in vivo. *J. Immunol.* **2007**, *179*, 186–194. [[CrossRef](#)]
10. Stienen, G.J.; Kiers, J.L.; Bottinelli, R.; Reggiani, C. Myofibrillar ATPase activity in skinned human skeletal muscle fibres: Fibre type and temperature dependence. *J. Physiol.* **1996**, *493*, 299–307. [[CrossRef](#)]
11. Barlow, C.H.; Chance, B. Ischemic areas in perfused rat hearts: Measurement by NADH fluorescence photography. *Science* **1976**, *193*, 909–910. [[CrossRef](#)] [[PubMed](#)]
12. Young, I.G.; Jaworowski, A.; Poulis, M.I. Amplification of the respiratory NADH dehydrogenase of Escherichia coli by gene cloning. *Gene* **1978**, *4*, 25–36. [[CrossRef](#)]
13. Raj, C.R.; Ohsaka, T. Electrocatalytic sensing of NADH at an in situ functionalized self-assembled monolayer on gold electrode. *Electrochem. Commun.* **2001**, *3*, 633–638.

14. Mayevsky, A.; Rogatsky, G.G. Mitochondrial function in vivo evaluated by NADH fluorescence: From animal models to human studies. *Am. J. Physiol. Cell Physiol.* **2007**, *292*, C615–C640. [[CrossRef](#)]
15. Mosmann, T. Rapid colorimetric assay for cellular growth and survival: Application to proliferation and cytotoxicity assays. *J. Immunol. Methods.* **1983**, *65*, 55–63. [[CrossRef](#)]
16. Barman, K.; Jasimuddin, S. Electrochemical detection of adenine and guanine using a self-assembled copper (II)–thiophenyl-azoimidazole complex monolayer modified gold electrode. *RSC Adv.* **2014**, *4*, 49819–49826. [[CrossRef](#)]
17. Sánchez-Tirado, E.; Salvo, C.; González-Cortés, A.; Yáñez-Sedeño, P.; Langa, F.; Pingarrón, J.M. Electrochemical immunosensor for simultaneous determination of interleukin-1 beta and tumor necrosis factor alpha in serum and saliva using dual screen printed electrodes modified with functionalized double-walled carbon nanotubes. *Anal. Chim. Acta* **2017**, *959*, 66–73. [[CrossRef](#)]
18. Sprules, S.D.; Hart, J.P.; Pittson, R.; Wring, S.A. Evaluation of a new disposable screen-printed sensor strip for the measurement of NADH and its modification to produce a lactate biosensor employing microliter volumes. *Electroanalysis* **1996**, *8*, 539–543. [[CrossRef](#)]
19. Yamada, K.; Hara, N.; Shibata, T.; Osago, H.; Tsuchiya, M. The simultaneous measurement of nicotinamide adenine dinucleotide and related compounds by liquid chromatography/electrospray ionization tandem mass spectrometry. *Anal. Biochem.* **2006**, *352*, 282–285. [[CrossRef](#)]
20. Song, J.; Kim, W.; Kim, Y.B.; Kim, B.; Lee, K. Time course of polyhexamethyleneguanidine phosphate-induced lung inflammation and fibrosis in mice. *Toxicol. Appl. Pharmacol.* **2018**, *345*, 94–102. [[CrossRef](#)]
21. Jain, P.; Chakma, B.; Patra, S.; Goswami, P. Hairpin stabilized fluorescent silver nanoclusters for quantitative detection of NAD⁺ and monitoring NAD⁺/NADH based enzymatic reactions. *Anal. Chim. Acta* **2017**, *956*, 48–56. [[CrossRef](#)] [[PubMed](#)]
22. Tiğ, G.A. Highly sensitive amperometric biosensor for determination of NADH and ethanol based on Au-Ag nanoparticles/poly(L-Cysteine)/reduced graphene oxide nanocomposite. *Talanta* **2017**, *175*, 382–389.
23. Selvarani, K.; Prabhakaran, A.; Arumugam, P.; Berchmans, S.; Nayak, P. 2D MoSe₂ sheets embedded over a high surface graphene hybrid for the amperometric detection of NADH. *Mikrochim. Acta* **2018**, *185*, 411. [[CrossRef](#)] [[PubMed](#)]
24. Vukojević, V.; Djurdjić, S.; Ognjanović, M.; Antić, B.; Kalcher, K.; Mutić, J.; Stanković, D.M. RuO₂/graphene nanoribbon composite supported on screen printed electrode with enhanced electrocatalytic performances toward ethanol and NADH biosensing. *Biosens. Bioelectron.* **2018**, *117*, 392–397. [[CrossRef](#)] [[PubMed](#)]
25. Meng, L.; Turner, A.P.; Mak, W.C. Positively-charged hierarchical PEDOT interface with enhanced electrode kinetics for NADH-based biosensors. *Biosens. Bioelectron.* **2018**, *120*, 115–121. [[CrossRef](#)]
26. Chamchoy, K.; Pakotiprapha, D.; Pumirat, P.; Leartsakulpanich, U. Application of WST-8 based colorimetric NAD (P) H detection for quantitative dehydrogenase assays. *BMC Biochem.* **2019**, *20*, 1–14. [[CrossRef](#)]
27. You, S.H.; Lim, H.D.; Cheong, D.E.; Kim, E.S.; Kim, G.J. Rapid and sensitive detection of NADPH via mBFP-mediated enhancement of its fluorescence. *PLoS ONE* **2019**, *14*, e0212061. [[CrossRef](#)]
28. Liu, R.; Wang, Y.; Du, N.; Jiang, D.; Ge, Q.; Wu, M.; Yu, H.; Xu, B. An electricalchemical method to detect the branch-chain aminotransferases activity in lactic acid bacteria. *Food Chem.* **2019**, *297*, 125035. [[CrossRef](#)]
29. Wilkening, S.; Schmitt, F.-J.; Lenz, O.; Zebger, I.; Horch, M.; Friedrich, T. Discriminating changes in intracellular NADH/NAD⁺ levels due to anoxicity and H₂ supply in *R. eutropha* cells using the Frax fluorescence sensor. *Biochim. Biophys. Acta (BBA)-Bioenerg.* **2019**, *1860*, 148062. [[CrossRef](#)]
30. Li, X.; Kan, X. A boronic acid carbon nanodots/poly(thionine) sensing platform for the accurate and reliable detection of NADH. *Bioelectrochemistry* **2019**, *130*, 107344. [[CrossRef](#)]
31. Thirupathi, M.; Lin, P.Y.; Chou, Y.T.; Ho, H.Y.; Wu, L.C.; Ho, J.A. Simple aminophenol-based electrochemical probes for non-enzymatic, dual amperometric detection of NADH and hydrogen peroxide. *Talanta* **2019**, *200*, 450–457. [[CrossRef](#)] [[PubMed](#)]
32. Chen, H.; Liu, X.; Yin, C.; Li, W.; Qin, X.; Chen, C. A dual-signal output ratiometric electrochemiluminescent sensor for NADH detection. *Analyst* **2019**, *144*, 5215–5222. [[CrossRef](#)] [[PubMed](#)]
33. Yang, H.; Hou, J.; Wang, Z.; Zhou, Q.; Xu, C. Porous PtAg nanoshells/reduced graphene oxide based biosensors for low-potential detection of NADH. *Mikrochim. Acta* **2020**, *187*, 544. [[CrossRef](#)] [[PubMed](#)]
34. Titoiu, A.M.; Necula-Petrareanu, G.; Visinescu, D.; Dinca, V.; Bonciu, A.; Mihailescu, C.N.; Purcarea, C.; Boukherroub, R.; Szunerits, S.; Vasilescu, A. Flow injection enzymatic biosensor for aldehydes based on a Meldola Blue-Ni complex electrochemical mediator. *Mikrochim. Acta* **2020**, *187*, 550. [[CrossRef](#)]
35. Liu, B.W.; Huang, P.; Wu, F.Y. Rapid visual detection for nitroreductase based on the copper ions-induced and NADH-mediated aggregation of gold-silver alloy nanoparticles. *Talanta* **2021**, *234*, 122681. [[CrossRef](#)]
36. Liu, B.W.; Huang, P.C.; Wu, F.Y. A novel light-controlled colorimetric detection assay for nitroreductase based on p-aminophenol-catalyzed and NADH-mediated synthesis of silver nanoparticles. *Anal. Methods* **2021**, *13*, 2223–2228. [[CrossRef](#)]
37. Moshirian-Farahi, S.S.; Zamani, H.A.; Abedi, M.R. Highly sensitive voltammetric determination of NADH based on N-CQDs decorated SnO₂/ionic liquid/carbon paste electrode. *Nanotechnology* **2021**. [[CrossRef](#)]
38. Wang, C.; Wang, T.; Li, Z.; Xu, X.; Zhang, X.; Li, D. An Electrochemical Enzyme Biosensor for Ammonium Detection in Aquaculture Using Screen-Printed Electrode Modified by Gold Nanoparticle/Polymethylene Blue. *Biosensors* **2021**, *11*, 335. [[CrossRef](#)]